

Article

Effect of Creep Aging Process on Microstructures and Properties of the Retrogressed Al-Zn-Mg-Cu Alloy

Yongqian Xu ^{1,2,3} and Lihua Zhan ^{2,3,4,*}

¹ Light Alloy Research Institute, Central South University, Changsha 410083, China; yongqian.xu@csu.edu.cn

² Collaborative Innovation Center of Advanced Nonferrous Structural Materials and Manufacturing, Central South University, Changsha 410083, China

³ State Key Laboratory of High-Performance Complex Manufacturing, Central South University, Changsha 410083, China

⁴ College of Mechanical and Electrical Engineering, Central South University, Changsha 410083, China

* Correspondence: yjs-cast@csu.edu.cn; Tel.: +86-731-88830254

Academic Editor: Nong Gao

Received: 31 May 2016; Accepted: 5 August 2016; Published: 17 August 2016

Abstract: The creep aging behaviors of retrogressed Al-Zn-Mg-Cu alloy were studied by uniaxial tensile creep tests at 140 °C. The effects of creep aging time and applied stress on microstructures and properties of the studied alloy were investigated by using transmission electron microscope (TEM), hardness, and corrosion resistance tests. Results show that the effects of the creep aging process on microstructures and properties are significant. The size of matrix precipitate (MPt), distance between MPts, width of precipitate-free zone (PFZ), and distance between grain boundary precipitates (GBPs) increase with the increase of creep aging time and applied stress. With the increase of creep aging time and applied stress, the corrosion resistance of the studied alloy improved. After creep aging for 20 h, the electrical conductivity varied with different applied stress from 35.99% to 37.24% International Annealed Copper Standard (IACS), and the exfoliation corrosion (EXCO) resistance increased to the corrosion rating of “EB”, which express slight surface corrosion. Compared with the traditional retrogression and re-aging process (RRA), the retrogression and creep aging process (RCA) can increase the MPt size, widen the precipitates distribution, narrow the PFZ width, and enhance the corrosion resistance while offering the hardness comparable to that of the RRA process.

Keywords: creep aging; retrogression; microstructures; corrosion resistance; Al-Zn-Mg-Cu alloy

1. Introduction

As a relatively new method for metal forming, creep age forming (CAF) is advantageous for manufacturing large, integral, and stiffened lightweight structures in light alloys for the aircraft and aerospace industries [1,2]. CAF simultaneously strengthens the part and changes its shape, resulting in a one-step forming and heat treatment process that can largely increase the mechanical properties. With the increasingly high performance requirements on the formed components, the aims of study on CAF should not only satisfy the needs of precision shape forming, but also meet the needs of high performance of the formed products [3–5]. However, controlling material performance is very difficult due to the presence of heavy interaction between creep and aging in the CAF process. For instance, the precipitates formed in aging will hinder the dislocation movement and thus hamper the creep. Meanwhile, the dislocation multiplication from creep deformation can provide more nucleation sites to promote aging precipitation. Especially, it is well-known that the heat-treatable high strength aluminum alloys have many heat treatment systems (such as T6, T73, and T74), and these systems may be used before CAF to obtain desired initial temper for controlling subsequent creep and aging process.

Aluminum alloys (7000 series) are extensively used in aeronautical applications, due to their very high strength [6]. One limitation of their use in the metallurgical state of highest strength (commonly called T6 or T651 temper) is the low resistance of these materials to structural corrosion (stress-corrosion cracking, exfoliation corrosion) [7,8]. In the past, the effects of the CAF process on microstructures and properties of aluminum alloy have been given attention [9]. Jeshvaghani et al. [9,10] investigated the effects of time and temperature on the microstructure of a 7075 aluminum alloy sheet during CAF, and observed the evolution of matrix and grain boundary precipitates. Guo et al. [11] found that the external elastic tensile stress promotes the formation of precipitates and shortens the aging period of an Al-Zn-Mg-Cu alloy. Lin et al. [12,13] studied the precipitate microstructures and corrosion resistances of 7075 aluminum alloy in the creep aging process, and found that with the increase of temperature and applied stress, the amount of the main strengthening η' and η phases increase and the exfoliation corrosion (EXCO) resistance first increases and then decreases. Fribourg et al. [14] investigated the evolution of precipitate microstructure during creep of an AA7449 aluminum alloy, and found that plastic deformation applied at the aging temperature induces an accelerated precipitate coarsening. Lin et al. [15] studied the effects of pretreatments on aging precipitates and corrosion resistance of a creep-aged 7075 aluminum alloy, and found that the intragranular aging precipitates are sensitive to retrogression pretreatment time, and suitable retrogression time vastly improves corrosion resistance of creep-aged alloy. It is noted that most of the above experimental materials are in the solution temper [5,11,14,16–18], and the effects of processing parameters on microstructures and properties of the retrogressed Al-Zn-Mg-Cu alloy in CAF are rarely reported.

Fortunately, the retrogression and re-aging (RRA) temper was developed to improve corrosion resistance without the loss of strength [19,20]. Referring to RRA process, we propose retrogression and creep aging process (RCA). A high strength Al-Zn-Mg-Cu alloy of 7B04 is taken as the case material in this paper, and this study aims to investigate the effects of RCA treatments on the precipitate microstructures and properties of 7B04-T651 aluminum alloy by using the uniaxial tensile creep tests under different CAF conditions. In addition, the traditional RRA experiments have been carried out in order to compare the aging precipitation and corrosion behaviors between the RCA and RRA processes.

2. Materials and Methods

2.1. Material and Heat Treatments

The present study was carried out on 7B04-T651 aluminum alloy, which means the as-received material had been subjected to solution-treatment at 471 °C for 1 h, quenched in cold water, followed by artificial aging treatment at 120 °C for 22 h, and then 2% pre-stretching to remove residual stress and quench distortion. The main compositional elements of as-received material are shown in Table 1. The bar samples (Figure 1) with a diameter of $\Phi 10$ mm and a gauge length of 100 mm were machined along the rolling direction.

Table 1. Chemical composition of 7B04 aluminum alloy (wt. %).

Al	Zn	Mg	Cu	Fe	Si	Cr
Bal.	5.97	2.48	1.51	0.16	0.07	0.16

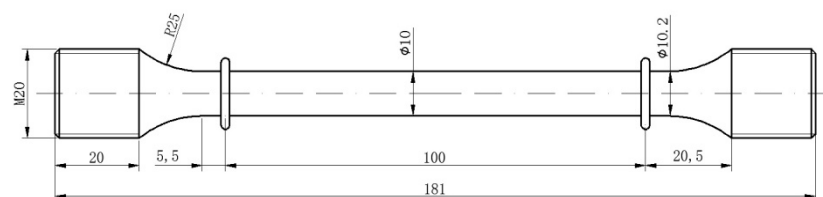


Figure 1. Geometry and size of samples (unit: mm).

Various treatment procedures of are shown in Figure 2. Figure 2a refers to the traditional creep aging process (CA) with solution temper [5]. Figure 2b,c represent the scheme of the various heat treatments used, i.e., the retrogression and re-aging (RRA) and the retrogression and creep aging (RCA) treatments, respectively. For retrogression pretreatment, the as-received material was subjected to a retrogression treatment held at 180 °C for 20 min in a furnace with the heating rate of 5 °C/min, and water quenched to room temperature. This state will be called hereafter RHT (retrogression heat treatment). The sample with RRA treatments was obtained from the retrogressed alloy by re-aging treatments. Re-aging heat treatments were carried out similarly to the initial partial heat treatment, namely 4, 12, and 20 h at 140 °C with a heating rate of 5 °C/min. Similar to the RRA treatment, the samples with the retrogression and creep aging (RCA) treatment included retrogression pre-treatment, and then creep aging for a range of stress levels at 140 °C.

Uniaxial tensile creep tests were carried out in a SUST-D5 creep testing machine made by ZHUHAI SUST ELECTRICAL EQUIPMENT CO., LTD. [21]. The creep aging tests were conducted using a specified 100 kN electronic creep aging testing machine with thermal environment furnace. The accuracies of heating and loading systems of the SUST-D5 creep test machine are 1 °C and 0.1 MPa, respectively. In creep aging tests, the sample was fitted and aligned in the middle of the furnace, and three thermocouples (K-type; Ni/Al-Ni/Cr) were tied in the top, middle, and bottom of the specimen gauge length. Firstly, the sample was heated to the experimental temperature at a heating rate of 5 °C/min and held for 20 min. Secondly, the extra stress was applied and held for 4, 12, and 20 h. Three different applied stresses (90, 180, and 270 MPa) were used in the experiments. Thirdly, the applied loading was released, and the samples naturally cooled down to room temperature in the furnace.

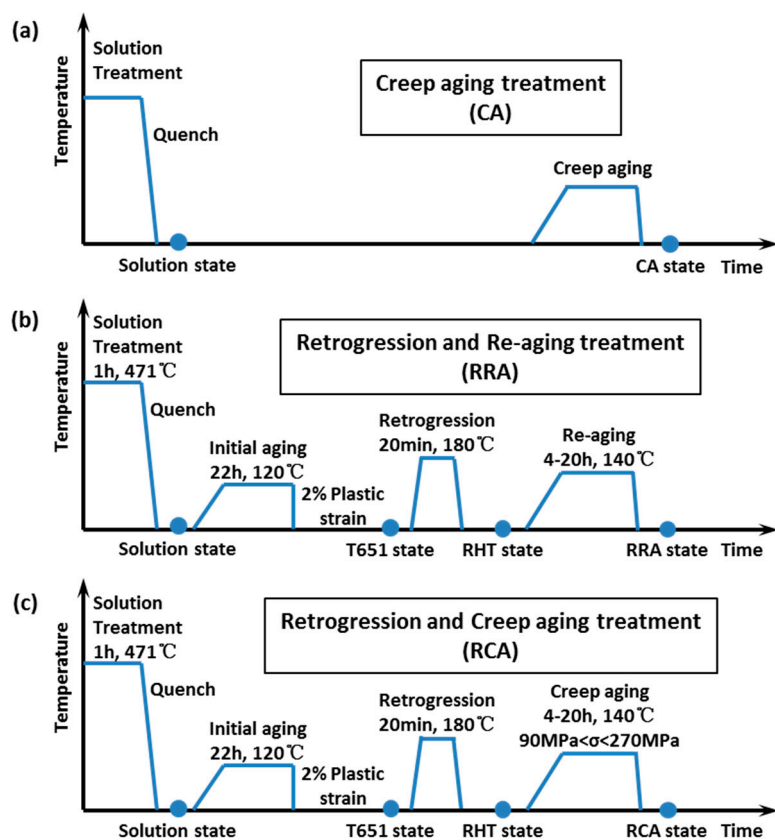


Figure 2. Scheme of the various heat treatments.

2.2. Microstructure Characterization

The microstructures of the retrogressed 7B04-T651 aluminum alloy during the creep aging process were characterized by transmission electron microscope (TEM, TecnaiG2 F20 S-TWIN TMP, Hillsboro, OR, USA) at 200 kV. The specimens for TEM were frictional thinned down to 60 μm , and cut to 3 mm disks. Then the disks underwent twin-jet electropolish in a solution of 30% perchloric acid and 70% ethanol at -25°C and 20 V.

The determination of microstructure characterization and its evolution with various CAF conditions is extremely important for the understanding of the final properties of the material. Figure 3 shows the sketch map of the microstructures of a typical Al-Zn-Mg-Cu alloy. Figure 3a,b shows the grain interior and grain boundary microstructures, respectively.

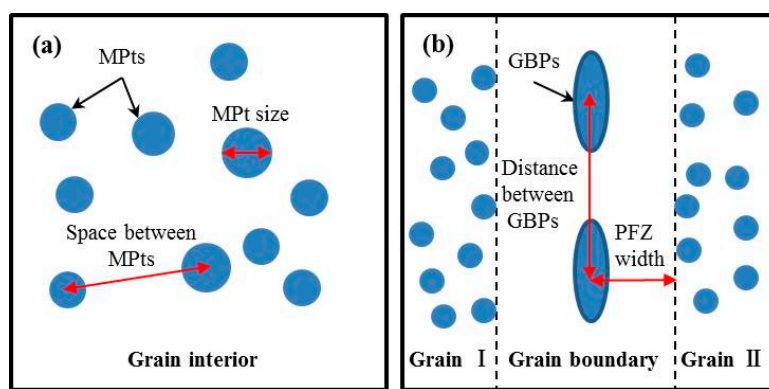


Figure 3. The sketch map of the microstructures of the typical Al-Zn-Mg-Cu alloy: (a) grain interior area of the field of view, FW_{GI}; (b) grain boundary area of the field of view, FW_{GB}.

Quantitative data of microstructures can be obtained using TEM statistical investigations and image analysis (Image J) following these steps [22]:

(1) Measurement of the apparent area (A) of each particle and determination of the matrix precipitate (MPt) size (M) using the equation:

$$M = \sqrt{4A/\pi} \quad (1)$$

(2) Calculation of the space between MPts (S), knowing the number of measurements for precipitates (N_{ppt}) and the area of the field of view (FW_{GI}):

$$S^{-1} = 0.5 \times \sqrt{N_{\text{ppt}}/\text{FW}_{\text{GI}}} \quad (2)$$

(3) Measurement of the width of grain boundary (W) in different positions and determination of the precipitate-free zone (PFZ) width (P) using the equation:

$$P = 0.5W \quad (3)$$

(4) Calculation of the distance between grain boundary precipitates (GBPs) (D), knowing the number of measurements for GBPs (N_{GBP}) and the grain boundary length (L) of the area of the field of view (FW_{GB}):

$$D = N_{\text{GBP}}/L \quad (4)$$

However, in some cases automatic identification and calculation of microstructures using the statistical software can make large errors due to the problem of edge definition. In order to avoid this problem, edge definitions were done manually by drawing close curves to enclose the regions, such as GBPs and MPts. Meanwhile, TEM observations reveal that the precipitates of heat-treated

Al-Zn-Mg-Cu alloy have different microstructures, and these microstructures are different from one grain to another. In order to describe the microstructure characteristics more precisely, a statistical method was used in the present study. For each sample, there were more than 300 measurements of MPts for determination of the average MPt size, 100 measurement of the width of grain boundary for determination of the average PFZ width, and 20 TEM micrographs for calculation of the mean space between MPts and distance between GBPs.

2.3. Hardness and Corrosion Resistance Tests

The properties of the creep-aged samples considered in this study were hardness, electrical conductivity, and EXCO resistance. The hardness tests were conducted by using a digital micro-Vickers hardness tester (HuaYin 200HVS-5, Shanghai, China) at a load of 3 kg applied for 15 s. Seven measurements were performed for each testing sample to calculate an average value of the hardness. The electrical conductivity measurement was performed by using the eddy current method according to the GB/T 12966-2008 [23]. The accelerated EXCO tests were carried out according to the ASTM G34-01 [24]. The sample was firstly degreased with ethanol after mirror polishing. The non-tested surfaces were protectively coated using a stop-off lacquer to avoid the crevice corrosion beneath the coating. The EXCO test solution was prepared as 4.0 M NaCl + 0.5 M KNO₃ + 0.1 M HNO₃. The solution temperature was 298 K, and the ratio of electrolyte volume to electrode surface area was 25 mL/cm². The corrosion surfaces of the samples after EXCO tests were observed by optical microscope (OLYMPUS BX60, Olympus, Tokyo, Japan).

3. Results and Discussion

3.1. TEM Observations of the 7B04 Aluminum Alloy with Various Heat Treatments

Figure 4 shows the TEM micrographs and corresponding Selected Area Electron Diffraction (SAED) pattern of the 7B04 aluminum alloy with various heat treatments. Figure 4a shows that the sample with T651 state has abundant fine matrix precipitates (MPts) and continuously distributed grain boundary precipitates (GBPs). The presence of GP zones and η' phases in the aluminum matrix was established by analyzing SAED pattern. By comparing between T651 and RHT state, it can be found that the size of precipitates is increased, the density of the MPts in RHT state is little reduced, and the GBPs in RHT state are slightly discontinuous (Figure 4b). Meanwhile, weak spots of η phase can be seen in the RHT state. According to the existing literature [25,26], in the retrogression stage, this dissolution results from the combination of the growth of the large (stable) precipitates and the dissolution of the smaller (unstable) ones. This means that retrogression makes the pre-precipitations in the matrix redissolve and grain boundary precipitation (GBP) coarsened. Figure 4c shows the growth of precipitates in retrogressed sample during creep aging process, resulting in the big-sized MPts and more discontinuous GBPs than in the RHT state. However, a great number of orientation relationships between the precipitates and the matrix can be observed, depending notably on the type of nucleation site (in the bulk, on dislocations, grain boundaries, dispersoids, etc.) [27]. Three different types of orientation relationships (which are noted as η_1 , η_2 , η_4 , etc.) can be distinguished from the location of their diffraction spots [14]. In this case, one can clearly distinguish the presence of the η_2 and η_4 variants.

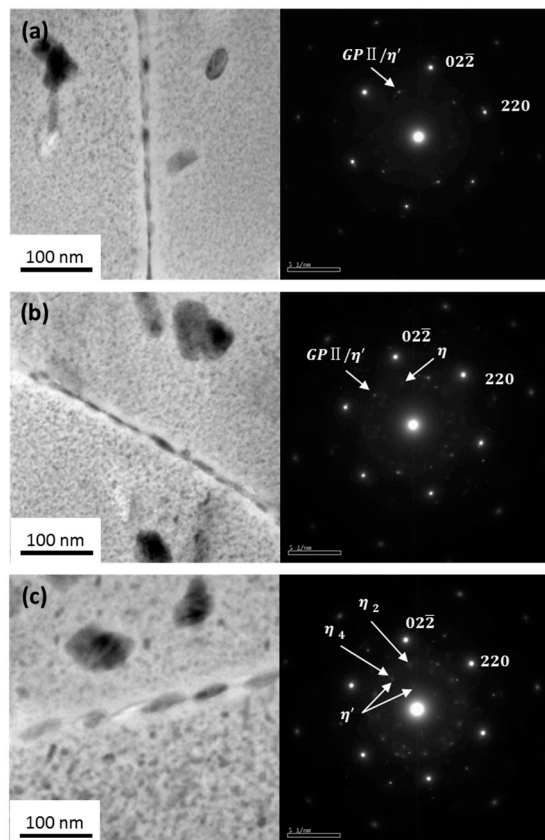


Figure 4. TEM micrographs and corresponding Selected Area Electron Diffraction pattern from $<111>$ Al projection of the 7B04 aluminum alloy with various states: (a) T651 state, as-received material; (b) retrogression heat treatment (RHT) state, 20 min at $180\text{ }^{\circ}\text{C}$; (c) retrogression and creep aging (RCA) state, 20 h at $140\text{ }^{\circ}\text{C}$ with applied stress of 180 MPa.

3.2. Effects of Creep Aging on Matrix Precipitate Microstructures

The evolution of matrix precipitate microstructures obtained by TEM statistical observations for the retrogressed 7B04 aluminum alloy during aging treatments at $140\text{ }^{\circ}\text{C}$ are shown in Figure 5. The effects of creep aging time on the MPt microstructures are significant. It proved that both the MPt size and the space between MPts increase with the increase of creep aging time. Deschanmps and Brechet [28] treated simultaneously three stages of precipitation (nucleation, growth, and coarsening). It can be deduced that the studied alloy experiences a combination of growth and coarsening mainly during the creep aging period time of 20 h. After creep aging for 20 h at $140\text{ }^{\circ}\text{C}$, the size of these MPt microstructures and the size of the space between MPts varied with applied stress from 5.31 to 7.12 nm and from 25.42 to 30.21 nm, respectively.

Obviously, the MPt microstructures are also greatly influenced by the applied stress during the creep aging test. With the increase of applied stress, the average MPt size and space between MPts increased sharply as shown in Figure 5a,b. At the end of creep aging tests, the RCA-270 MPa sample has the largest average MPt size and space between MPts, and the values are approximately 21.5% and 13.1% higher than those of the creep-aged sample with RCA-90 MPa temper. The main reason is that the greater applied stress can generate more dislocations in the aluminum matrix, and these dislocations increase the kinetics of the aging process [29]. Compared with the RRA process, the RCA process can increase the MPt size and the distance between MPts. It means that the precipitate-hardening of RCA process is different from that of RRA process.

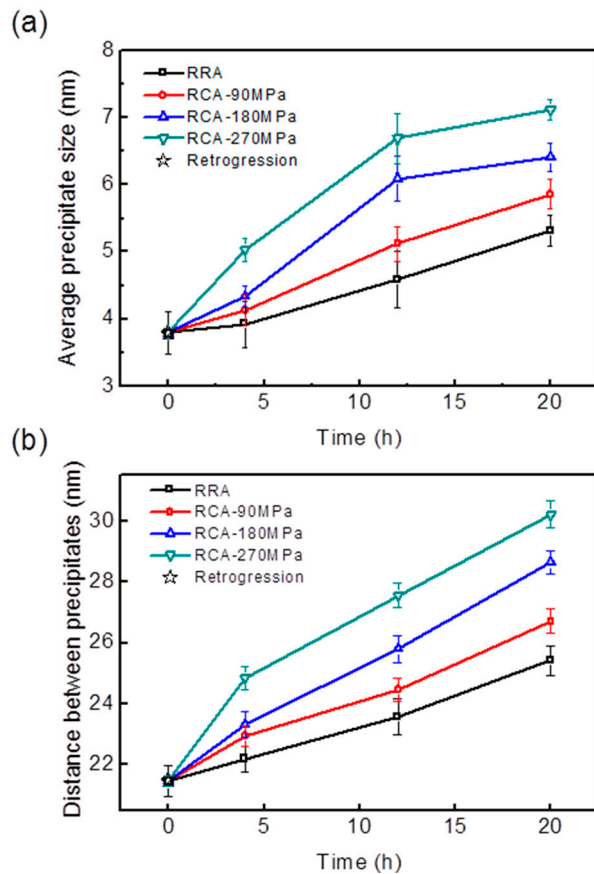


Figure 5. Evolutions of matrix precipitate (MPt) microstructures of the retrogressed 7B04-T651 aluminum alloy during aging treatments: (a) the average MPt size; (b) the mean space between MPts.

3.3. Effects of Creep Aging on Grain Boundary Microstructures

The evolution of grain boundary microstructures for the retrogressed 7B04 aluminum alloy during aging treatments at 140 °C are shown in Figure 6. It can be found that, for all creep-aged samples, the PFZ width and the distance between GBPs increase with the increase of creep aging time. The grain boundary microstructures under relatively high applied stress (270 MPa) are the most affected by the creep aging time. With the increase of creep aging time, in RCA-270 MPa samples, the average PFZ width widened from 12.84 nm to 28.06 nm, and the mean distance between GBPs rapidly increased from 11.96 nm to 84.31 nm.

From Figure 6, it can be shown that the PFZ width and the distance between GBPs increase with the increase of applied stress. At the end of creep aging test, the PFZ width is slightly wider vary with different applied stress from 26.43 nm to 28.06 nm (Figure 6b). With the increase of applied stress, the distance between GBPs in creep aged for 20 h samples increase from 66.34 nm to 84.31 nm (Figure 6a). Moreover, there is a great difference between the RCA and RRA on grain boundary microstructures of the 7B04-T651 aluminum alloy. Compared with the RRA process, the RCA process can disperse the distance between GBPs and narrow the PFZ width. Grain boundaries act as sinks of solute and vacancies, thus causing precipitate concentrates on the surroundings of this region. The growth and coarsening of GBPs are accompanied by the formation of PFZ. Lin et al. [13] has shown that creep aging process can produce an abundance of dislocations at the grain boundary, which supplies the nucleation cores for precipitates. Once the nucleation is formed, the precipitates will take advantage of the elastic strain energy to increase in size. For RRA sample, few nucleation cores of precipitates appear and the pre-existing precipitates grow quickly during the aging process. Therefore, the PFZ width in RRA sample is larger than that in RCA samples.

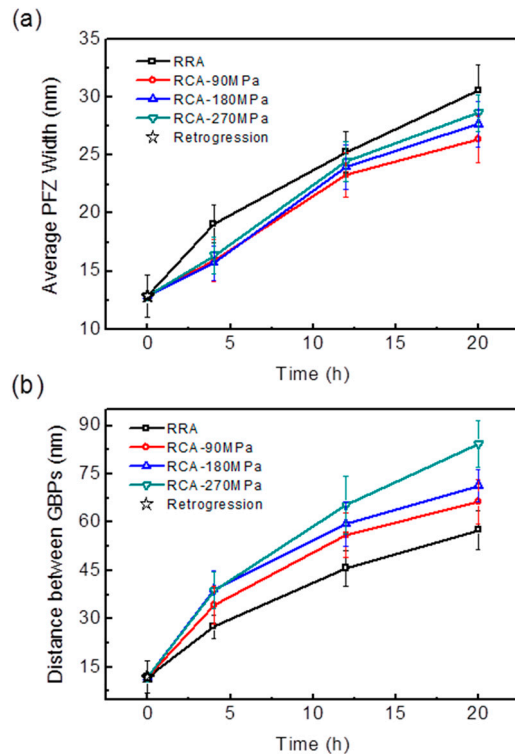


Figure 6. Evolutions of grain boundary microstructures of the retrogressed 7B04-T651 aluminum alloy during aging treatments: (a) the average width of GBPs; (b) the mean distance between GBPs.

3.4. Effects of Creep Aging on Hardness

Figure 7 displays the evolution of hardness of the retrogressed 7B04-T651 aluminum alloy during various aging treatments at 140 °C. From the hardness curves, it can be seen that, for any applied stress level, the hardness of the retrogressed alloy reaches a peak value after aging for 4 h, and then decreases with aging time. The hardness is mainly attributed to the interaction between precipitates and dislocations, namely precipitate strengthening. Combining Figures 5 and 7, it is implied that the optimal precipitate size for strength is 3.92, 4.13, 4.34, and 5.03 nm for the studied alloy with the stress of 0, 90, 180, and 270 MPa at 140 °C, respectively. Orowan strengthening mechanism [30] shows that the precipitate hardening increases with the increase of MPt size for the shearable precipitates, and decreases with the increase of space between MPts for the unshearable precipitates. Results from the current study showed both of the average MPt size and the mean space between MPts increased with the increase of aging time (Figure 5), suggesting that precipitate hardening of the retrogressed 7B04-T651 aluminum alloy is dominated by shear mechanism in the first (less than 4 h at 140 °C) and then is dominated by bypass mechanism. Because of the space between MPts of the creep-aged AA7B04-T651 is the largest with the stress of 270 MPa (Figure 5b), so the hardness of the creep aged AA7B04-T651 is the lowest with the stress of 270 MPa.

The hardness slightly decreased in RCA samples with the increase of applied stress during the creep aging process as shown in Figure 7. After creep aging for 20 h, these RCA samples' hardness is approximately 0.5%–1.5% smaller than the RRA sample. It indicated that, due to fine precipitates in the retrogressed sample, the RCA process could offer the strength comparable to that of the traditional RRA process. Essentially, this occurs due to the nonsymmetric nature of the size-strength relationship (i.e., large nonshearable precipitates all have the same strength, while for the shearable precipitates, the strength is a function of the MPt size) [31,32].

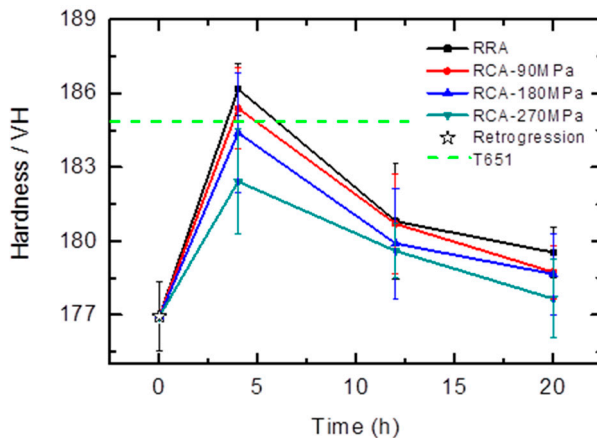


Figure 7. Hardness of the studied aluminum alloy during various aging treatments at 140 °C.

3.5. Effects of Creep Aging on Corrosion Resistance

The electrical conductivity of aluminum alloy may serve as an indicator of stress crack corrosion (SCC) resistance [33]. Figure 8 shows the evolution of electrical conductivity for the retrogressed 7B04-T651 aluminum alloy during various aging treatments at 140 °C. It can be found that, for any CAF conditions, the electrical conductivity of alloy increases with time during creep aging. Due to dissolution of precipitates, which makes electron movement easier, the electrical conductivity increases from 31.8% IACS in retrogressed sample to 35.99%–37.24% IACS in varied RCA samples after aging for 20 h. As shown in Figure 8, the electrical conductivity increased with the increase of applied stress. It demonstrated that SCC resistance enhanced with the increase of creep aging time and applied stress. Compared with the RRA process, the RCA process can significantly increase the electrical conductivity. The RCA-270 MPa sample has the maximum conductivity, which is greater than that of the RRA sample by about 7%.

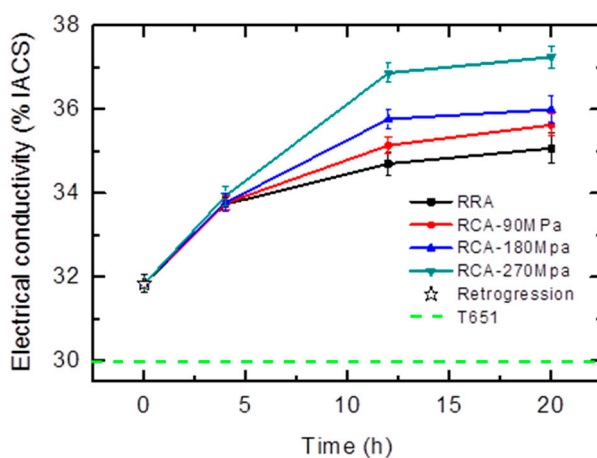


Figure 8. Electrical conductivity of the studied alloy during various aging treatments at 140 °C.

In the exfoliation corrosion (EXCO) tests, the corrosion products gradually break away from the samples surface. Figure 9 show the corroded surface morphologies of the retrogressed 7B04-T651 aluminum alloy with various aging treatments after EXCO solution for 48 h. From Figure 9a, it can be seen that a large amount of corroded layers are peeled off from the metal surface in the retrogressed sample. For the RRA sample, some cracks and slightly corroded layers can be found on the metal surface (Figure 9b). In contrast, the RCA samples have a slighter surface corrosion compared to the

RRA sample, and some tiny surface cracks can be observed (Figure 9c–e). Moreover, it can be found that the number of microcracks is slightly reduced in RCA samples with the increase of applied stress.

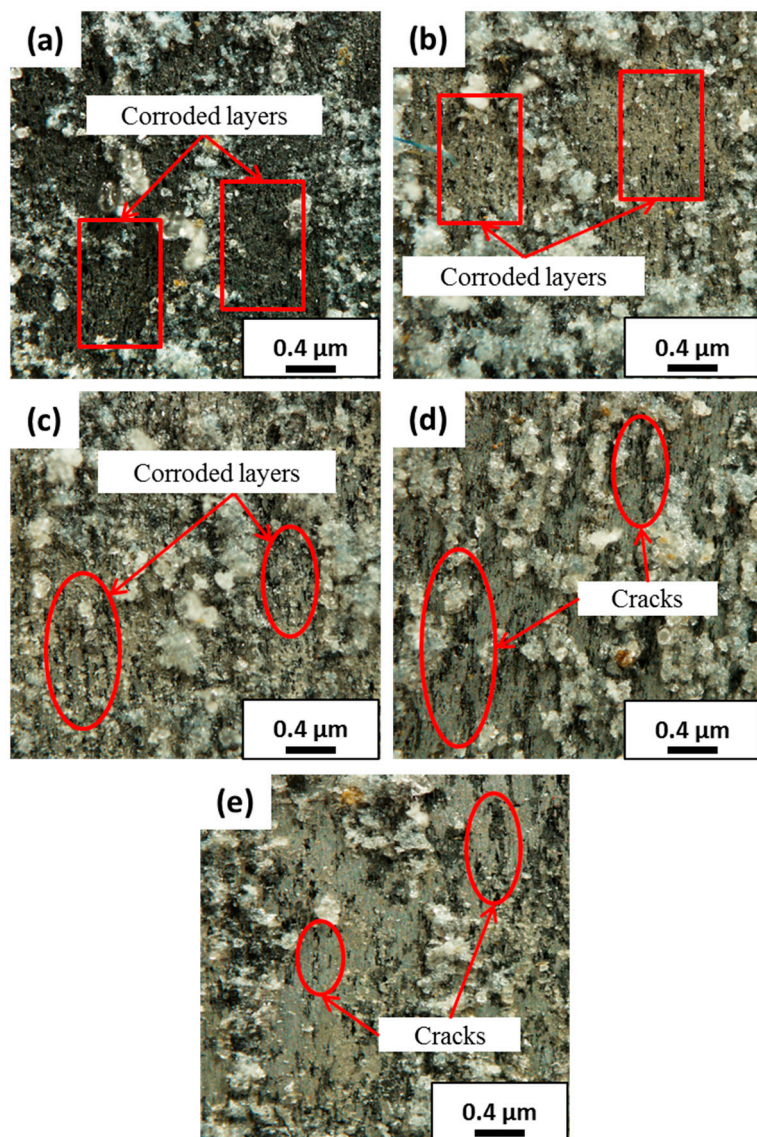


Figure 9. Exfoliation corrosion (EXCO) morphologies of the creep aged 7050 aluminum alloy with various initial tempers: (a) retrogression; (b) retrogression and re-aging (RRA); (c) RCA-90 MPa; (d) RCA-180 MPa; (e) RCA-270 MPa.

The corrosion degree can be described by the EXCO ratings according to different corrosion stages. The total EXCO behavior is commonly classified into six stages including no obvious corrosion (expressed as N), slight pitting corrosion (P), growth of pitting corrosion (EA), slight surface corrosion (EB), lifted surface layers and blisters (EC), and severe peeled off layers and metal loss (ED). In the same corrosion stage, the “−” and “+” signs indicate that the corrosion behavior is relatively minor and serious, respectively. Based on the observations of surface morphologies at different times during EXCO tests, Table 2 shows the EXCO evolutions of the 7B04 aluminum alloy with various heat treatments. It is observed that the EXCO rating decreases with the aging time. When the retrogressed 7B04 aluminum alloy is placed in a corrosive environment, its relatively continuous GBPs are noted as being anode to the aluminum matrix (Figure 6b), and thus it is susceptible to EXCO and SCC. For the aged RRA and RCA samples, their discontinuous GBPs have large spaces to each other. The anodic

corrosion channel is cut off [13,34], so these samples have less corrosion susceptibility, especially the RCA temper. Furthermore, it is found that exfoliation corrosion susceptibility is decreased with the increase of applied stress. This indicates that the corrosion resistance is slightly enhanced by the increased applied stress.

Table 2. The exfoliation corrosion rating of 7B04 aluminum alloy.

Applied Stress (MPa)	Aging Time (h)	EXCO Rating
As-received (T651)		ED
Retrogression		ED ⁻
RRA(0 MPa)	4 h	ED ⁻
	12 h	EC
	20 h	EC ⁻
RCA-90 MPa	4 h	EC ⁺
	12 h	EC
	20 h	EB
RCA-180 MPa	4 h	EC ⁺
	12 h	EC ⁻
	20 h	EB
RCA-270 MPa	4 h	EC ⁺
	12 h	EB
	20 h	EB

It is well-known that (1) Precipitate-free zones (PFZ) are the main paths for intergranular corrosion. Grain boundary with continuous precipitates becomes a susceptive anode channel, which results in the galvanic reaction between the anodic precipitates and aluminum matrix; (2) There are potential differences between the precipitate-free zones and aluminum matrix, which leads to the anodic dissolution of the grain boundary precipitates [35,36]. It is suggested that the grain boundary microstructures are responsible for the corrosion resistance. From Figure 6, the width of PFZ and the distance between GBPs are both increase with the increase of creep aging time and applied stress. It indicated that the corrosion resistance is more sensitive to the distance between GBPs rather than the width of PFZ. In addition, compared with the traditional retrogression and re-aging process (RRA), the retrogression and creep aging process (RCA) can widen the GBPs' distribution and narrow the PFZ width (Figure 6). Thus, the corrosion resistance in RCA-treated samples is better than that in RRA-treated ones.

4. Conclusions

The effects of creep aging on microstructures and properties of retrogressed 7B04-T651 aluminum alloy under CAF conditions were studied. The main conclusions can be summarized as follows:

(1) The matrix precipitate (MPt) size and the space between MPts increase with the increase of creep aging time and applied stress. With the increase of creep aging time and applied stress, the width of precipitate free zone (PFZ) broaden and the distance between grain boundary precipitates (GBPs) increased.

(2) Related to the matrix precipitate microstructures, the hardness increases in the first 4 h and then decreases with aging time, suggesting that precipitate hardening of the studied alloy is dominated by shear mechanism in the first and then is dominated by bypass mechanism.

(3) The corrosion resistance of the studied alloy improve with the increase of creep aging time and applied stress. After creep aging for 20 h, the electrical conductivity varies with applied stress from 35.99% IACS to 37.24% IACS and the EXCO resistance increased to the corrosion rating of "EB".

(4) Compared with the RRA process, the retrogression and creep aging (RCA) process can increase the average MPt size, disperse the precipitate distribution, narrow the PFZs width and improve the corrosion resistances while offering the hardness comparable to that of the RRA process.

Acknowledgments: The authors would like to thank the Key Program of National Natural Science Foundation of China (Grant No. 51235010), the Project of Innovation-driven Plan in Central South University (Grant No. 2015CX002), the National Key Basic Research Development Plan Funded Project of China (Grant No. 2014CB046602) and Research Fund for the Doctoral Program of Higher Education of China (Grant No. 20120162110003) for their financial support.

Author Contributions: Y.X. and L.Z. conceived and designed the study. Y.X. performed the experiments and wrote the paper. L.Z. reviewed and edited the manuscript.

Conflicts of Interest: The authors declare no conflict of interest.

References

1. Zhan, L.H.; Lin, J.G.; Dean, T.A. A review of the development of creep age forming: Experimentation, modelling and applications. *Int. J. Mach. Tools Manuf.* **2011**, *51*, 1–17. [[CrossRef](#)]
2. Du, X.D. Study on ageing and creep of Al-0.1Zr alloy. *Mater. Sci. Eng. A* **2006**, *432*, 84–89. [[CrossRef](#)]
3. Ho, K.C.; Lin, J.; Dean, T.A. Modelling of springback in creep forming thick aluminum sheets. *Int. J. Plast.* **2004**, *20*, 733–751. [[CrossRef](#)]
4. Jeunechamps, P.-P.; Ho, K.C.; Lin, J.; Ponthot, J.-P.; Dean, T.A. A closed form technique to predict springback in creep age-forming. *Int. J. Mech. Sci.* **2006**, *48*, 621–629. [[CrossRef](#)]
5. Zhan, L.H.; Lin, J.; Dean, T.A.; Huang, M.H. Experimental studies and constitutive modelling of the hardening of aluminium alloy 7055 under creep age forming conditions. *Int. J. Mech. Sci.* **2011**, *53*, 595–605. [[CrossRef](#)]
6. Dursun, T.; Soutis, C. Recent developments in advanced aircraft aluminium alloys. *Mater. Des.* **2014**, *56*, 862–871. [[CrossRef](#)]
7. Puiggali, M.; Zielinski, A.; Olive, J.M.; Renauld, E.; Desjardins, D.; Cid, M. Effect of microstructure on stress corrosion cracking of an Al-Zn-Mg-Cu alloy. *Corros. Sci.* **1988**, *40*, 805–819. [[CrossRef](#)]
8. Marlaud, T.; Baroux, B.; Deschamps, A.; Chemin, J.L.; Henon, C. Understanding the compromise between strength and exfoliation corrosion in high strength 7000 alloys. *Mater. Sci. Forum.* **2006**, *519–521*, 455–460. [[CrossRef](#)]
9. Jeshaghani, R.A.; Emami, M.; Shahverdi, H.R.; Hadavi, S.M.M. Effects of time and temperature on the creep forming of 7075 aluminum alloy: Springback and mechanical properties. *Mater. Sci. Eng. A* **2011**, *528*, 8795–8799. [[CrossRef](#)]
10. Jeshaghani, R.A.; Shahverdi, H.R.; Hadavi, S.M.M. Investigation of the age hardening and operative deformation mechanism of 7075 aluminum alloy under creep forming. *Mater. Sci. Eng. A* **2012**, *552*, 172–178. [[CrossRef](#)]
11. Guo, W.; Yang, M.; Zheng, Y.; Zhang, X.S.; Li, H.; Wen, X.Y.; Zhang, J.W. Influence of elastic tensile stress on aging process in an Al-Zn-Mg-Cu alloy. *Mater. Lett.* **2013**, *106*, 14–17. [[CrossRef](#)]
12. Lin, Y.C.; Jiang, Y.Q.; Chen, X.M.; Wen, D.X.; Zhou, H.M. Effect of creep-aging on precipitates of 7075 aluminum alloy. *Mater. Sci. Eng. A* **2013**, *588*, 347–356. [[CrossRef](#)]
13. Lin, Y.C.; Jiang, Y.Q.; Zhang, X.C.; Deng, J.; Chen, X.M. Effect of creep-aging processing on corrosion resistance of an Al-Zn-Mg-Cu alloy. *Mater. Des.* **2014**, *61*, 228–238. [[CrossRef](#)]
14. Fribourg, G.; Bréchet, Y.; Chemin, J.L.; Deschamps, A. Evolution of precipitate microstructure during creep of an AA7449 T7651 aluminum alloy. *Metall. Mater. Trans.* **2011**, *42*, 3934–3940. [[CrossRef](#)]
15. Lin, Y.C.; Zhang, J.L.; Liu, G.; Liang, Y.J. Effects of pre-treatments on aging precipitates and corrosion resistance of a creep-aged Al-Zn-Mg-Cu alloy. *Mater. Des.* **2015**, *83*, 866–875. [[CrossRef](#)]
16. Li, C.; Wan, M.; Wu, X.D.; Huang, L. Constitutive equations in creep of 7B04 aluminum alloys. *Mater. Sci. Eng. A* **2010**, *527*, 3623–3629. [[CrossRef](#)]
17. Zhan, L.H.; Li, Y.G.; Huang, M.H. Effects of process parameters on mechanical properties and microstructures of creep aged 2124 aluminum alloy. *Trans. Nonferr. Met. Soc. China* **2014**, *24*, 2232–2238. [[CrossRef](#)]
18. Junior, P.R.C.; Neto, C.D.; Wade, D.A. Essai d'une table non-vibrante par enregistrement du mouvement brownien d'un galvanomètre. *Mater. Res.* **2014**, *17*, 603–611.

19. Ning, A.L.; Liu, Z.Y.; Peng, B.S.; Zeng, S.M. Redistribution and re-precipitation of solute atom during retrogression and reaging of Al-Zn-Mg-Cu alloys. *Trans. Nonferr. Met. Soc. China* **2007**, *17*, 1005–1011. [[CrossRef](#)]
20. Feng, C.; Liu, Z.Y.; Ning, A.L.; Zeng, S.M. Retrogression and re-aging treatment of Al-9.99%Zn-1.72%Cu-2.5%Mg-0.13%Zr aluminum alloy. *Nonferr. Met. Soc. China* **2006**, *16*, 1163–1170. [[CrossRef](#)]
21. Oliveira, A.F., Jr.; de Barros, M.C.; Cardoso, K.R.; Travessa, D.N. The effect of RRA on the strength and SCC resistance on AA7050 and AA7150 aluminium alloys. *Mater. Sci. Eng. A* **2004**, *379*, 321–326. [[CrossRef](#)]
22. Hashmi, S. Comprehensive Materials Processing. *Creep Age Form. Model. Charact.* **2014**, *2*, 150–155.
23. GB/T 12966-2008. The method for determining aluminum alloys conductivity using eddy current. General Administration of Quality Supervision, Inspection and Quarantine of the People's Republic of China: Beijing, China, 2008.
24. ASTM G 34-01. Standard test method for exfoliation corrosion susceptibility in 2XXX and 7XXX series aluminum alloys (EXCO test). American Society for Testing and Materials: West Conshohocken, PA, USA, 2013.
25. Marlaud, T.; Deschamps, A.; Bley, F.; Lefebvre, W.; Baroux, B. Evolution of precipitate microstructures during the retrogression and re-ageing heat treatment of an Al-Zn-Mg-Cu alloy. *Acta Mater.* **2010**, *58*, 4814–4826. [[CrossRef](#)]
26. Wang, Y.L.; Pan, Q.L.; Wei, L.L.; Li, B.; Wang, Y. Effect of retrogression and reaging treatment on the microstructure and fatigue crack growth behavior of 7050 aluminum alloy thick plate. *Mater. Des.* **2014**, *55*, 857–863. [[CrossRef](#)]
27. Degischer, H.P.; Lacom, W.; Zahra, A.; Zahra, C.Y. Decomposition processes in an Al-5%Zn-1%Mg alloy. II. Electronmicroscopic investigations. *Z. Metallkd.* **1980**, *71*, 231–238.
28. Deschamps, A.; Livet, F.; Bréchet, Y. Influence of predeformation on ageing in an Al-Zn-Mg alloy—I. Microstructure evolution and mechanical properties. *Acta Mater.* **1998**, *47*, 281–292. [[CrossRef](#)]
29. Poole, W.J.; Seter, J.A.; Skjervold, S.; Waterloo, G. A model for predicting the effect of deformation after solution treatment on the subsequent artificial aging behavior of AA7030 and AA7180 alloys. *Metall. Mater. Trans. A* **2000**, *31*, 2327–2338. [[CrossRef](#)]
30. Ashby, M.F. Results and consequences of a recalculation of the frank-read and the orowan stress. *Acta Metall.* **1966**, *14*, 679–681. [[CrossRef](#)]
31. Deschamps, A. Analytical Techniques for Aluminum. In *Handbook of Aluminum of Volume 2: Alloy Production and Materials Manufacturing*; Totten, G.E., MacKenzie, D.S., Eds.; CRC Press: Boca Raton, FL, USA, 2003; pp. 160–169.
32. Chen, J.F.; Zhen, L.; Jiang, J.T.; Yang, L.; Shao, W.Z.; Zhang, B.Y. Microstructures and mechanical properties of age-formed 7050 aluminum alloy. *Mater. Sci. Eng. A* **2012**, *539*, 115–123. [[CrossRef](#)]
33. Knight, S.P.; Pohl, K.; Holroyd, N.J.H.; Birbilis, N.; Rometsch, P.A.; Muddle, B.C.; Goswami, R.; Lynch, S.P. Some effects of alloy composition on stress corrosion cracking in Al-Zn-Mg-Cu alloys. *Corros. Sci.* **2015**, *98*, 50–62. [[CrossRef](#)]
34. Li, J.F.; Birbilis, N.; Li, C.X.; Jia, Z.Q.; Cai, B.; Zheng, Z.Q. Influence of retrogression temperature and time on the mechanical properties and exfoliation corrosion behavior of aluminium alloy AA7150. *Mater. Charact.* **2009**, *60*, 1334–1341. [[CrossRef](#)]
35. Xiao, Y.P.; Pan, Q.L.; Li, W.B.; Liu, X.Y.; He, Y.B. Influence of retrogression and re-aging treatment on corrosion behaviour of an Al-Zn-Mg-Cu alloy. *Mater. Des.* **2011**, *32*, 2149–2156. [[CrossRef](#)]
36. Sun, X.Y.; Zhang, B.; Lin, H.Q.; Zhou, Y.; Sun, L.; Wang, J.Q.; Han, E.H.; Ke, W. Correlations between stress corrosion cracking susceptibility and grain boundary microstructures for an Al-Zn-Mg alloy. *Corros. Sci.* **2013**, *77*, 103–112. [[CrossRef](#)]

